APPENDIX A: Hydroclimatic reconstructions in the Lower Basin: Water year streamflow reconstruction of the Virgin River

by Kiyomi Morino and David Meko,
Laboratory of Tree-Ring Research, The University of Arizona

Table of Contents

A.1 Study Basin

The Virgin River watershed drains an area of about 15,000 km^2 (3.7 million acres). The river is about 270 km (170 miles) long, originating in the Pink Cliffs region at the southern boundary of the Markagunt Plateau, located in the northeast corner of the watershed, and terminating to the southwest in the Overton arm of Lake Mead. The watershed spans a wide range of elevations, from 365 – 3050 m (1,200 – 10,000 ft) and contains a wide variety of physiographic provinces, from desert to conifer and aspen forest. Surface water is dominated by snowmelt with minor contributions from groundwater and springs at Littlefield Springs and Petrified Springs. The watershed is comprised of 3 sub-watersheds: the Upper Virgin (HUC:15010008), the Lower Virgin (HUC:15010010) and Fort Pearce Wash (HUC:15010009) (Figure A-1).

A.2 Data

A.2.1 Hydrologic Data.

Monthly average streamflow from for the Virgin River at Littlefield (USGS 09415000) were downloaded from the US Geological Survey (http://waterdata.usgs.gov/). Data span a period beginning in October 1929 and ending in September 2011. At the Virgin River at Littlefield USGS gage, the mean daily discharge for water years over the period of record is 6.88 cms (243 cfs) (USGS 2012b). The highest water year mean was 23.36 cms (825 cfs) in 2005; the lowest was 2.83 cms (100 cfs) in 1991. Average water year runoff is 216.97 mcm (175.9 kaf). Reconstructed flows for the Colorado River at Lees Ferry, Arizona, from Meko et al. (2007) were downloaded from NOAA's WDC for Paleoclimalogy (http://www.ncdc.noaa.gov/paleo/). Reconstructed flows for the Gila River were provided by D. Meko.

A.2.2 Precipitation Data

Precipitation variations were characterized with PRISM (Precipitation-elevation Regressions on Independent Slopes Model) data (Gibson et. al 2002). Monthly PRISM data, 1900-2010, for the continental US were downloaded from the PRISM site (http://prism.oregonstate.edu/products/). Data pertaining to the Virgin River basin (Upper and Lower basins) were "clipped" from the larger dataset using a script written in MatLab ™. Volume of precipitation (MCM) over the entire basin was computed.

A.2.3 Hydroclimatology

Precipitation in the Virgin River watershed is bimodal but dominated by cool-season (October through April) moisture (Figure A-2). The importance of snowmelt is readily apparent in the peak streamflow months of March, April and May. June and July have the lowest streamflows. The effect of summer rains does not appear to manifest until August.

Scatterplots of flow on seasonal-total precipitation suggest flow responds primarily to cool-season precipitation (Figure A-3). Correlation of water year streamflow with

October through April precipitation is 87% (N = 78). These data suggest the relationship between precipitation and streamflow is linear. Warm-season precipitation (July through September) shows no relation with annual streamflow (r =0.09, N=78); nevertheless, these rains are important for recharging soil moisture. There appears to be a weak relationship between May-June rains and streamflow despite low levels of precipitation during this season. Saturated, or near-saturated, soil moisture following snowmelt likely account for the sensitive response of the basin to even small amounts of precipitation.

The level of interannual variability varies for precipitation (*volP*) and streamflow (*Q*) records. Precipitation shows generally high levels of variability throughout the period of record apart from slightly reduced levels in the 1940s (Figure A-4). Streamflow shows low-moderate variability in flow from the mid-1940s through the 1960s. After 1970, several wet years punctuate a series of annual flows measuring at or below average. The wettest water year on record was 2005 with an annual flow of 736.5 MCM (597 KAF); the driest water year was in 1991 with an annual flow of 89.5 MCM (72.5 KAF). Trend for the period of record, as described by a least-square-fit straight line of the hydrologic variable on water year, is positive for both precipitation and flow, but for neither series is the slope of the trend-line statistically significant. There is no trend in the ratio series *Q*/*P*.

A.2.4 Tree-Ring Data.

See *Hydroclimatic Reconstructions in the Lower Basin of the Colorado River, METHODS* for details regarding tree-ring data standardization.

Tree-ring data for this reconstruction consisted of measured ring-widths. These were obtained from the International Tree-Ring Data Bank (ITRDB) (http://www.ncdc.noaa.gov/paleo/treering.html) and from new sites collected for this study (Table A-1). The reconstruction generated in this study made use of 13, from an initial pool of 17, chronologies located in and around the Virgin River basin. Sites were selected with the criteria that the species be moisture-sensitive and the data cover at least the period 1700-1970. The 1700 cutoff ensured that at least three centuries of reconstructed streamflow data could be later analyzed for patterns of temporal variability; the 1970 cutoff ensured a reasonably long period (~40 years) for calibration of flow with tree rings in the reconstruction model.

A.3 Methods

Analysis of reconstructions utilized a variety of statistical tools. Correlation analysis and significance-testing of correlations follow Snedecor and Cochran (1989), with adjustment as needed for autocorrelation (Dawdy and Matalas 1964). Assessment of low-frequency fluctuations included smoothing by evenly-weighted moving averages (Panofsky and Brier 1958) and Gaussian filters (Mitchell et al. 1966). Covariation of the Virgin River with: 1) the Colorado River and 2) the Gila River as a function of frequency was summarized by cross-spectral analysis (Bloomfield 2000). More details on this technique can be found in Meko and Woodhouse (2005).

A.3.1 Reconstruction Model

See *Hydroclimatic Reconstructions in the Lower Basin of the Colorado River, METHODS* for details regarding methods employed in single-site reconstructions.

A.4 Results and Discussion

A.4.1 Reconstruction modeling

Tree-Ring Chronology Development

The set of 13 tree-ring chronologies passing the screening for sample depth and correlation with flow are listed in Table A-1. Their site locations are marked by green shaded triangles on the map in Figure A-1. The common period is 1557 – 1971. Four of the thirteen sites extend out to at least 2008. The first year of the reconstruction was dictated by the earliest year when the predictor chronologies showed adequate subsample signal strength (SSS>0.85), 1496.

Descriptive statistics showed that all chronologies have near-zero autocorrelation and negative skew (Table A-2). Skew is significantly (p<0.01) negative for all but three chronologies. The near-zero autocorrelation is expected, as these are residual chronologies (Cook et al. 1990b).

Single-Site Reconstruction

The SSR models explain 19 to 44 percent of the variance of flow in the calibration period, which ranges in length from 42 to 78 years for the 13 sites (Table A-3). Calibration periods start with 1930, the first year of available flow data, but end in different years (1971 to 2008) depending on the collection data of the chronology. All models have some skill of verification, as indicated by an RE-statistic above zero.

The final selected smoothing parameter, α , for the SSR models ranges from 0.45 to 0.80. As previously described, the variation in selected α reflects differences in curvature of the statistical relationship between flow and tree-ring index where values closer to 1.0 indicate a more linear relationship between flow and tree-ring index.

Recalibration and Reconstruction

Summary statistics of the loess models used to recalibrate the scores of PC#1 of the SSRs into final estimates of flow are listed in Table A-4. The percentage of streamflow variance explained by the models ranged from 43 percent for Model A and 71 percent for Model B. All three models show skill in reconstructing streamflow, reflected by positive RE statistics for cross-validation.

Figure A-5 shows the loadings of each of the sites that comprise each of the 3 models. Model B was developed from the largest number of sites, thirteen. The majority are located to the east of the basin, near the headwaters region, with one site located to the north, Panaca Summit, and one site located to the south of the basin, Little Wolf Pass. Models A and C which comprise the earlier and latter portions of the reconstruction, respectively, consist of sites located near the headwaters. Model A, developed from three sites, shows markedly higher loadings for a single site,Yovimpa; whereas, Model C,

developed from 4 sites, shows higher loadings for two sites, Lower Henderson and Allen Canyon.

Differences between observed and reconstructed streamflow for the two models are evident in Figure 6. All three models track low flows reasonably well. However, 1968 stands out in that it is overestimated by all three models; in Models A and C by significant amounts. For the period prior to 1970, Models B and C do a slightly better job tracking high flows, namely in 1832, 1941, 1952 and 1969 but see 1958. After 1970, Model C provides a better fit for a few of the high-flow years, eg., 1983 and 1995, but also overestimates flows in several years putting it out of phase with the observed record.

Uncertainty

The validation statistics mirror the calibration R^2 in showing the superior accuracy of Model B over Models A and C (Table A-4). The RMSE of cross-validation for Model B is 61.1 MCM which is just under half of the standard deviation of observed flows for 1930-2010. Analysis of residuals in Model B indicates dependence in variance of reconstruction error on magnitude of reconstructed flow for both positive and negative residuals (Figure A-7). The absolute value of residuals increases with magnitude of reconstructed flow. For positive residuals, the median value of residuals almost doubles from the lowest to middle tercile of reconstructed flow; for negative residuals, the median absolute value of residuals nearly quadruples from the lowest to middle tercile of reconstructed flow. Assessment of such patterns is speculative, however, given the small sample size of the residuals.

A.4.2 Reconstructed streamflows

Annual flows

Annual reconstructed flows, 1496-2010, are plotted in Figure A-8A along with a baseline at the long-term median of 193 MCM (156 KAF) to facilitate identification of wet years and dry years. The annual reconstructed flows have a mean of 220 MCM (178 KAF), are positively skewed (skew =1.22, $p<0.01$), not significantly autocorrelated ($r_1=0.025$, $p>0.05$), and slightly wet relative to the observed flows, whose 1930-2010 mean is 215 MCM (174 KAF). The relative wetness is not surprising since the observed flows include one of the longest droughts (1950s) and do not begin until after the well-documented wet initial decades of the 20th century.

The frequency of dry years reaches an all-time high in the latter part of the 1800s with more than two-thirds of the years below the median (Figure A-8B). Indeed, from about 1850 to 1900, there were extended periods of flow below the median. A similarly high frequency of dry years characterize much of the 1700s. In contrast, the 1500s was relatively wet with "dry" years (years below the median) occurring less than half the time in a 30-year sliding window.

Moving averages

Reconstructed flow anomalies for periods of length 5-50 years are summarized graphically in Figure A-9. The baseline for comparison is the 1930-2010 reconstructed

mean. Red "flames" denote periods of dry conditions. As window length increase, there is a tendency for moving averages to more closely approximate the baseline mean. For window sizes greater than 30 years, the mid-20th century stands out as a very dry period. Comparable but not as severe droughts occurred in the late 1500s and mid-1600s. For decadal scale droughts, less than 15 or so years, there are several events that occur in the 1600s and occur periodically throughout the 1700s and 1800s. The series of severe droughts in the 1700s and 1800s are separated by extremely wet periods.

Covariation with Colorado River and Gila River

The series selected for comparison with the Virgin River were the Colorado River (Meko et al 2007) and the Gila River (Meko). Both the Colorado and Gila River reconstructions were truncated to match the shorter Virgin River reconstruction. For both comparisons, cross-spectral analysis was conducted over the full common period, as well as over two sub-periods, from the beginning of the common period to 1700 and from 1700 to the end of the common period. Split-sample analysis of covariation was carried out to verify the stability of relationship over the full period.

Virgin River and Colorado River

Smoothed time series plots of the two reconstructions show generally close agreement in timing of low-frequency fluctuations (Figure A-10A). The 21-year Gaussian filter used to smooth the series in Figure A-10A emphasizes multi-decadal fluctuations. Joint drought, defined as smoothed series simultaneously in their lowest quartile, occurs 10 times in the last 500 years; 7 of these occur after 1700. The 1950s and an interval in the early 1600s are the longest of these joint droughts. A cross-spectral analysis of the two reconstructions supports strong agreement over frequencies over most of the spectrum (Figure A-10B-D). The individual spectra are slightly low-frequency with no significant peaks but relatively high variance at wavelengths between five and ten years. The Virgin River spectrum also has relatively high variance at wavelengths between three and five years. Coherency, analogous to correlation as a function of frequency, is significant for medium to low-frequencies but not high frequencies, i.e., for wavelengths less than ~3 years (Figure A-10D). The phase spectrum shows no evidence of out-of-phase behavior in the two series (Figure A-10E). The small departure from zero-phase at lower and higher frequencies can be disregarded as having no practical importance as the corresponding offset in the time domain is less than a year.

Split-sample analysis of covariation indicates that the coherency between the two series is stronger after 1700 (Figure A-11B). During this later period, frequency variations for wavelengths around five years are significant. Prior to 1700, coherency is not significant at any frequency (Figure A-11A). During this early period, relatively high variance occurs at wavelengths of about three and ten years.

Virgin River and Gila River

Smoothed time series plots of the two reconstructions show generally close agreement in timing of low-frequency fluctuations (Figure A-12A). High synchronicity of these smoothed curves is particularly evident during the period after 1700 with the Gila River showing higher amplitude fluctuations. Joint drought, defined as smoothed series

simultaneously in their lowest quartile, occurs 8 times in the last 500 years; 6 of these occur after 1700. The 1950s-60s and an interval in the late 1500s are the longest of these joint droughts. A cross-spectral analysis of the two reconstructions supports agreement at all frequencies (Figure A-12B-D). The individual spectra have no significant peaks but relatively high variance at wavelengths of >~15 years (Figure A-12B, C). The Virgin River spectrum also has relatively high variance at wavelengths of between three and ten years (Figure A-12B); whereas, the Gila River also has relatively high variance at wavelengths of about ten years (Figure A-12C). Coherency is significant across the full frequency-range of the spectrum, excluding frequencies of about 0.3 yr^{-1} (Figure A-12D). The phase spectrum shows no evidence of out-of-phase behavior in the two series (Figure A-12E). The small departure from zero-phase at lower frequencies can be disregarded as having no practical importance as the corresponding offset in the time domain is less than a year.

Split-sample analysis of covariation indicates that the coherency between the two series is stronger after 1700 (Figure A-13B). During this later period, coherencies at multiple wavelengths from ~2 to ~20 years are significant. Prior to 1700, coherency is almost significant at low frequencies but is otherwise not significant over the rest of the spectrum (Figure A-13A). During this early period, relatively high variance occurs at frequencies similar to the ones with significant coherence during the period after 1700. Wavelengths of ~10 years are an exception. For this wavelength, there is significant coherency after 1700 but essentially no coherency before 1700.

A.5 Conclusions

The time series of reconstructed streamflow of the Virgin River reveals several interesting features of the dynamics of drought in this basin. The most severe drought in the 20th century occurred in the 1950s and 1960s. Relative to historic droughts, it was longer-lasting but lower in magnitude. A series of droughts in the 1700s were shorter in duration but much more severe; moreover, each was separated by extremely wet periods. The mid-1500s stand out in terms of the low frequency of dry years.

Covariation of the Virgin River with the Colorado River and the Gila River indicate different coherency patterns over time and space. In both cases, the Virgin River showed higher coherence with each river during the latter part of the reconstruction, i.e., after 1700. Significant covariation, however, occurred at different frequencies and with different magnitudes for comparisons between the Virgin River and each river. The strongest coherency occurred between the Virgin and Gila Rivers during the post-1700 period. Several significant peaks occurred throughout the spectrum from high to low frequency. One of the striking features of streamflow dynamics for all three of these rivers was the quasi-regular, decadal-length periodicity during the 1700s.

A potential limitation of this reconstruction is the distribution and number of sites. The majority of sites were clustered to the east of the Virgin River watershed. These sites were not located within the watershed boundary but were able to successfully portray fluctuations in water availability because they were situated near the headwaters of the

Virgin River. Additional sites within the headwaters region could serve to sharpen the hydrologic signal and provide a more skillful reconstruction as would new or updated chronologies from other areas of the watershed that are runoff producing. Moreover, bolstering sample depth would likely improve the reconstruction's ability to track streamflow fluctuations in the earlier and latter portions of the reconstruction which is currently comprised of linear combinations of three and four sites, respectively.

TABLES

Table A-1. List of site chronologies.

N[1]	Site[2]	Species[3]	Location[4] Lat	Lon	El(m)	Period[5]
1	Little Wolf Pass	PIED	36.8	-113.7	1800	1546-1971
2	Kaibab Plateau	PIED	36.6	-112.1	2100	1482-1976
3	Paria Plateau	PIED	36.8	-112.1	1860	1481-1975
4	Upper Henderson	PSME	37.7	-111.9	3000	1259-2010
5	Yovimpa	PSME	37.5	-112.5	2750	1436-1998
6	Deer Springs	PIED	37.3	-112.2	2200	1477-2000
7	Lower Henderson	PIED	37.6	-112.0	2100	1507-2010
8	Skutumpah	PIED	37.5	-112.1	1900	1406-2000
9	Panaca Summit	PIMO	37.8	-114.2	2103	1556-1982
10	Red Rock	PIPO	37.4	-112.1	2134	1300-2011
11	Coal Bench	PIED	37.6	-112.0	2100	1555-2000
12	Round Valley	PIED	37.4	-111.9	2000	1561-1999
13	Allen Canyon	PIPO	37.7	-111.8	2164	1557-2011

1 Site number
2 Site name
3 Species code: PIED is *Pinus edulis*, PSME is *Pseudotsuga menzeisii*, PIMO is *Pinus monophylla*, and PIPO is *Pinus ponderosa*
4 Latitude and longitude in decimal degrees, elevation in m above sea level
5 Start and end year of chronology, after trimming as described in text

Table A-2. Chronology basic statistics.

						Replication and Common Signal[4]		
N	Length[1]	Mean	Stdev	Skew[2]	r(1)[3]	#Cores	SSS	EPS
1	376(161)	1.007	0.216	-0.26*	-0.05	3-18	0.85	0.82-0.96
2	369(187)	0.999	0.244	-0.35**	-0.09	4-26	0.88	0.85-0.97
3	371(152)	1.008	0.272	-0.37**	-0.03	3-23	0.87	0.84-0.97
4	611(166)	0.998	0.115	-0.52**	-0.08	6-50	0.91	0.89-0.98
5	517(154)	0.995	0.229	-0.46**	-0.05	4-30	0.85	0.82-0.97
6	503(166)	0.999	0.215	-0.52**	-0.05	3-30	0.87	0.85-0.98
7	419(189)	1.003	0.221	-0.48**	-0.07	3-28	0.86	0.83-0.98
8	367(151)	0.999	0.198	-0.47**	-0.07	3-18	0.88	0.83-0.96
9	322(150)	0.999	0.263	-0.21	-0.08	3-38	0.86	0.83-0.97
10	432(233)	1.000	0.147	-0.85**	0.00	5-15	0.85	0.77-0.90
11	395(176)	0.998	0.230	-0.50**	-0.06	3-14	0.88	0.83-0.95
12	408(150)	1.000	0.212	-0.41**	-0.10	3-23	0.89	0.85-0.97
13	400(225)	1.001	0.185	-0.27*	0.07	4-12	0.90	0.84-0.94

1 Length of site chronology, with minimum segment length in parentheses
2 Skewness (*,** denote significance at 0.05, 0.01 level)
3 First-order autocorrelation (*,** denote r(1) significantly different from zero at 0.05, 0.01 level)
4 Range in number of cores, minimum value of subsample signal strength, and range in expressed population signal

Table A-3. Summary of single-site loess models.

	Calibration[2]			Validation[3]		
N[1]	Period	α	V	RMSE	RE	RMSE	Group[4]
1	1930-1971	0.55	0.44	73.3	0.35	81.0	B
2	1930-1976	0.65	0.28	84.4	0.16	92.9	B
3	1930-1975	0.60	0.29	84.0	0.18	92.0	B
4	1930-2008	0.70	0.23	115.4	0.18	120.2	ABC
5	1930-1998	0.45	0.40	94.5	0.32	102.0	AB
6	1930-1998	0.70	0.25	105.1	0.21	109.6	AB
7	1930-2008	0.55	0.35	106.3	0.29	112.3	BC
8	1930-2000	0.40	0.37	95.4	0.30	102.0	B
9	1930-1982	0.60	0.35	88.5	0.28	95.1	B
10	1930-2008	0.70	0.19	118.2	0.15	122.8	BC
11	1930-2000	0.50	0.28	102.6	0.20	109.4	B
12	1930-1999	0.50	0.27	103.1	0.20	109.9	B
13	1930-2008	0.35	0.38	103.8	0.28	112.8	BC

1 Site number, names cross-listed on Table 1
2 Calibration statistics: N=period for estimation of loess curve,
α=loess smoothing parameter,V=variance-explained decimal fraction,
RMSE=root-mean-square error of calibration
3 Validation statistics from leave-1-out cross-validation:
RE=reduction of error statistic, RMSE=root-mean-square error
4 Subperiod reconstruction groups each chronology is used in

Table A-4. Summary of sub-period reconstruction models.

			Calibration[4]			Validation[5]	
N[1]	Period[2]	p[3]	α	V	RMSE	RE	RMSE
A	1496-1998	3	0.20	0.43	92.0	0.32	102.1
B	1661-1971	13	0.35	0.71	52.6	0.63	61.1
C	1611-2010	4	0.30	0.47	95.9	0.34	107.8

1 Sub-period model number
2 Starting and ending years of sub-period
3 Number of chronologies
4 Calibration statistics: α=loess smoothing parameter, V=variance-explained decimal fraction, RMSE=root-mean-square error of calibration
5 Validation statistics from leave-1-out cross-validation: RE=reduction of error statistic, RMSE=root-mean-square error

FIGURES

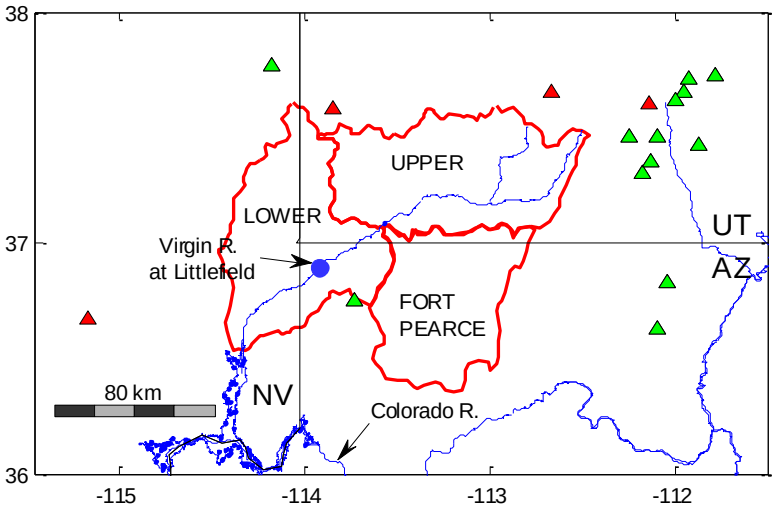

Figure A-1. Site map.

Map showing Virgin sub-watersheds and tree-ring site locations. Tree-ring sites that passed screenings for sample depth and correlation with streamflow are denoted by green triangles. Tree-ring sites that did not pass screenings are denoted by red triangles.

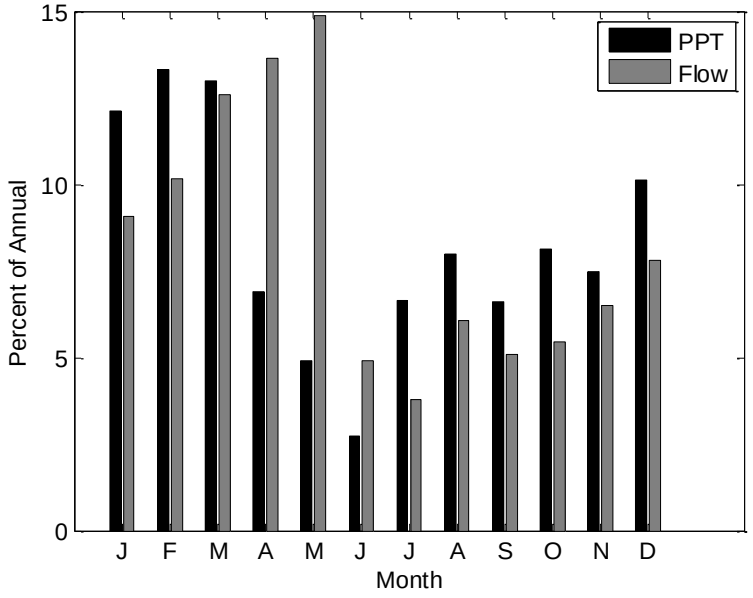

Figure A-2. Monthly basin precipitation and streamflow.

Bar charts summarizing annual distribution of monthly basin precipitation and streamflow. Streamflow data is from Virgin River at Littlefield gage. Precipitation is total volume of precipitation over the entire watershed; data from PRISM. Period of analysis is 1930-2008.

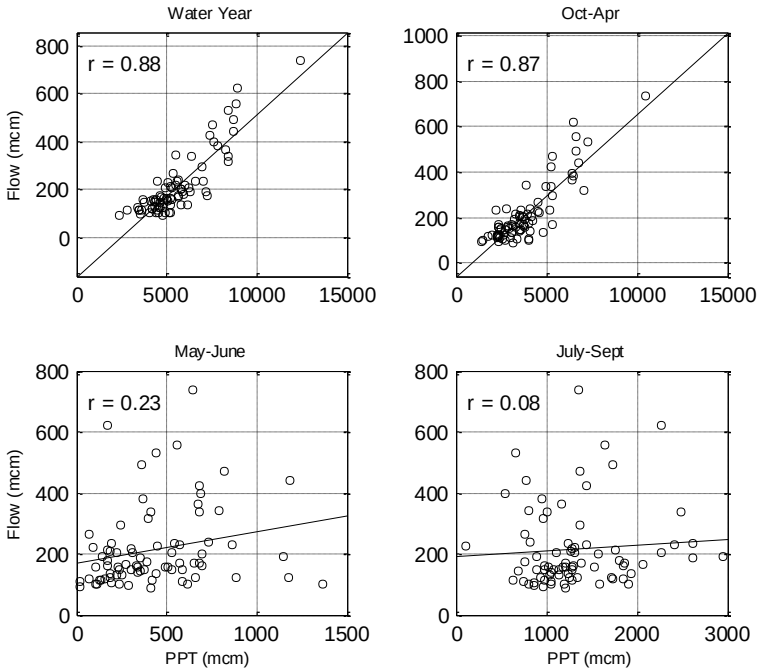

Figure A-3. Relationships between annual flow on seasonal precipitation.

Scatterplots showing relationship between water year streamflow and precipitation for water year, winter (October through April), early summer (May through June) and lay summer (July through September). Streamflow data is from Virgin River at Littlefield gage. Precipitation is total volume of precipitation over the entire watershed; data from PRISM. Analysis period is 1930 to 2008.

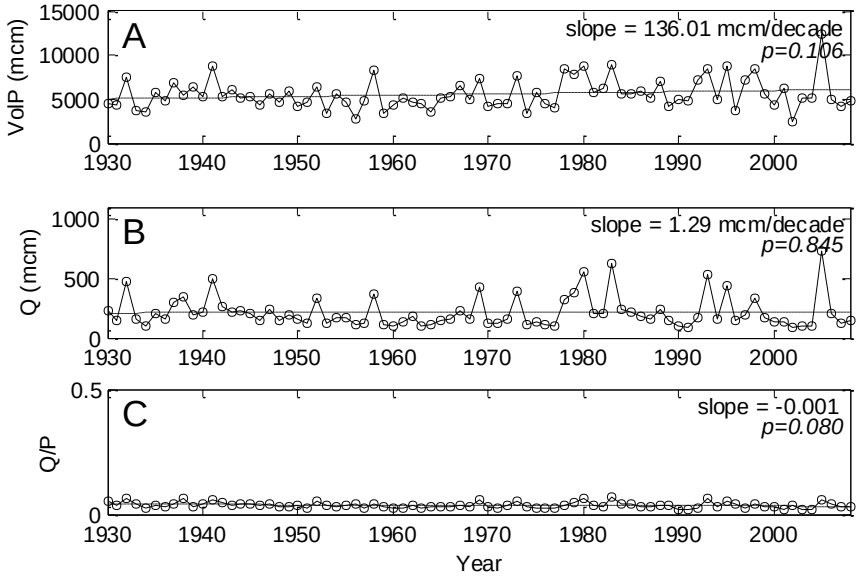

Figure A-4. Time trends in precipitation, flow, and the ratio of flow to precipitation.

(A) Total volume of precipitation over the Virgin River basin for water year. (B) Streamflow on the Virgin River at Littlefield for water year in million cubic meters (MCM). (C) Ratio of flow to precipitation volume. Least squares fit straight line for 1930-2008 is plotted for each series, and slope and its significance are annotated.

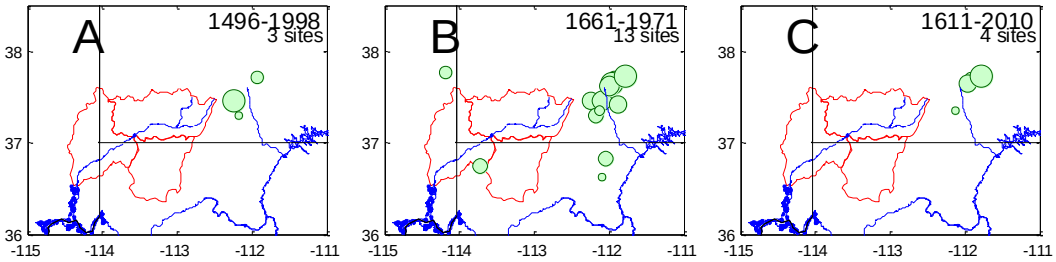

Figure A-5. PC loadings.

Tree-ring site locations for sub-period reconstruction models. Models A, B and C coded as in Tables 4. Symbol sizes reflect magnitude of loadings of sites on PC#1 of SSRs.

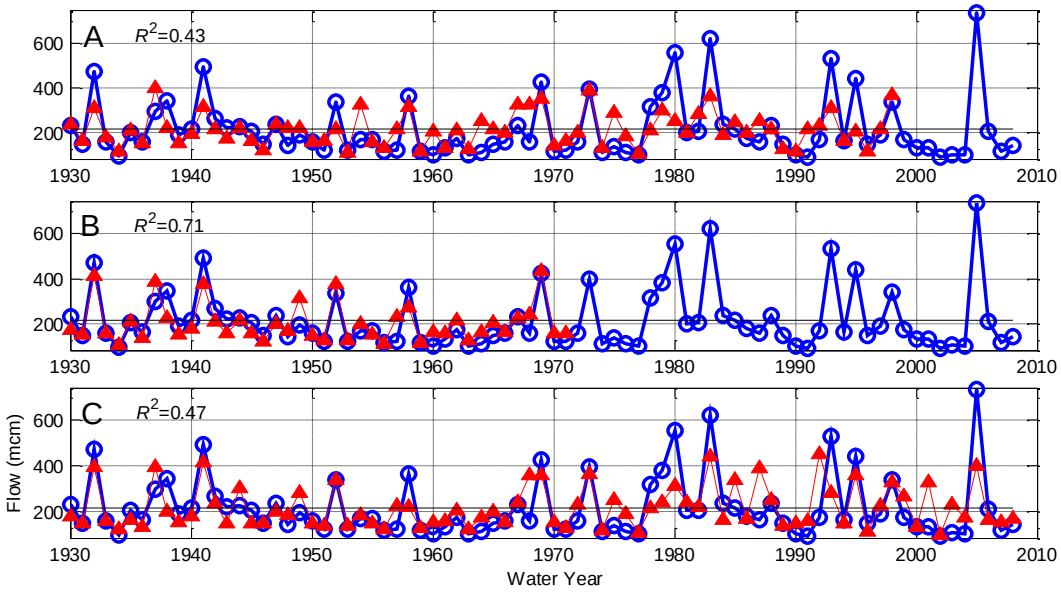

Figure A-6. Agreement of observed and reconstructed streamflow.

Agreement of observed and reconstructed flows for three sub-period models (as coded in Table 4). Annotated at upper left is the variance explained by the model. Horizontal line is the observed mean flow for the period, 1930-2008.

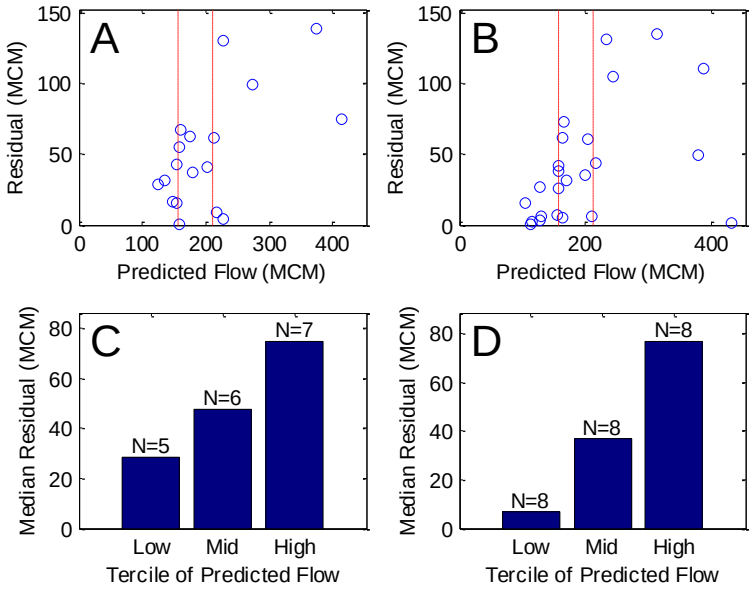

Figure A-7. Estimated reconstruction uncertainty.

Estimated reconstruction uncertainty for Model B. Terciles of reconstructed (predicted) flow, 1930-1971, are marked by vertical dashed lines in A and B. (A) Positive cross-validation residuals as function of predicted flow. (B) Absolute value of negative cross-validation residuals as function of predicted flow. (C) Median positive cross-validation residual for different terciles of reconstructed flow. (D) Median of absolute values of negative cross-validation residuals for terciles of reconstructed flow.

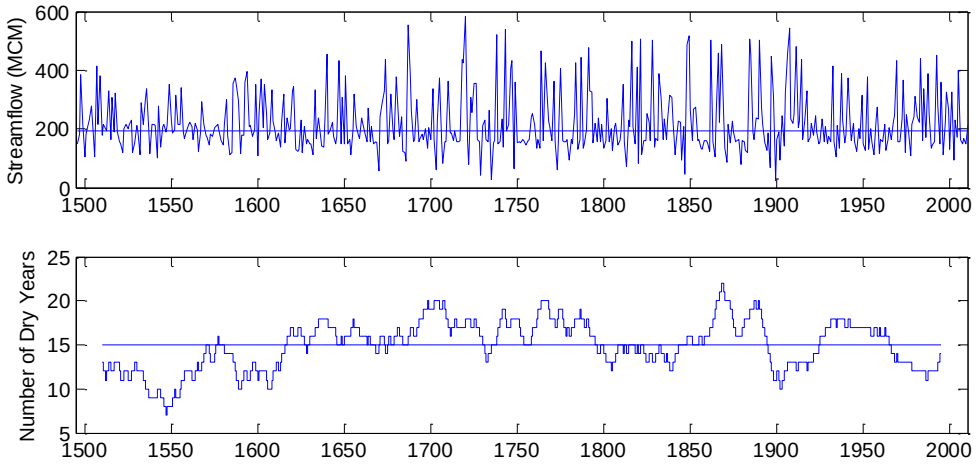

Figure A-8. Time plots of annual reconstructed streamflow.

Time plots of annual reconstructed years and dry-year frequency. (A) Reconstructed flows, 1496-2010, and dry year threshold (horizontal line) at median. (B) Frequency of dry years in centered 30-year moving window. The median reconstructed flow is 193 MCM (156 KAF), or 87 percent of the long-term mean, 220 MCM (178 KAF). Horizontal line in (B) is expected number of dry years in 30-year window.

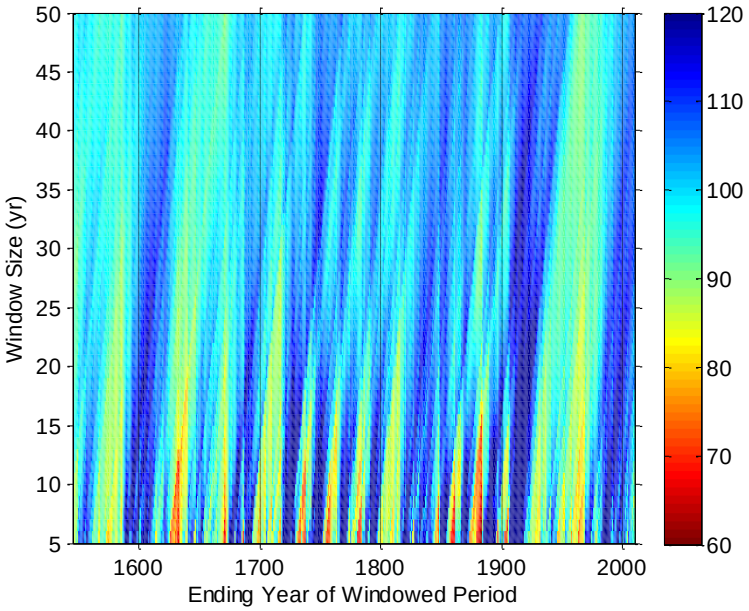

Figure A-9. Color-mapped running means of reconstructed streamflow.

Running means of length 5, 6, …50 years ending in years 1545-2010 are mapped as a percentage of the 1930-2010 reconstructed mean. Color mapping is truncated at 60 and 120 percent of the mean: flows lower than 60 percent are mapped as the darkest red and flows greater than 120 percent as the darkest blue.

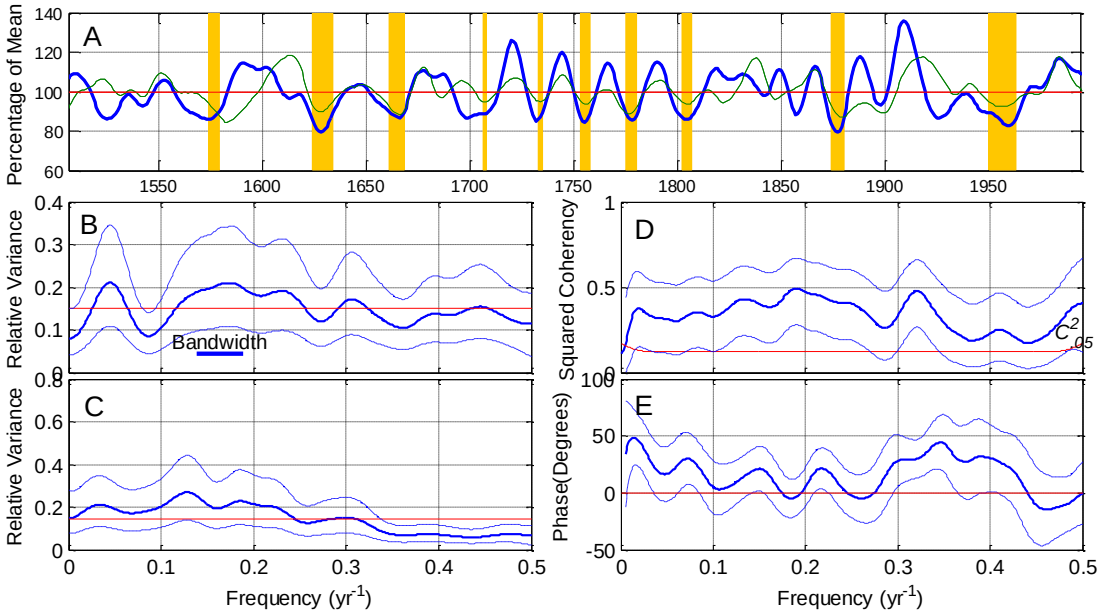

Figure A-10. Covariation of Virgin and Colorado River reconstructed flows, 1496-2005

(A) Smoothed reconstructed flow series as percentage of long-term mean. Intervals with smoothed series simultaneously below 0.25 quantile shaded. Thick blue line is Virgin River; thin green line is Colorado River. (B) Spectrum of Virgin. (C) Spectrum of Colorado. (D) Coherency spectrum from cross-spectral analysis of Virgin and Colorado. (E) Phase spectrum from the cross-spectral analysis. Smoothing in (A) by 21-year Gaussian filter. Confidence intervals (dashed) on spectral and cross-spectral plots are 95%. Line labeled $C^2_{.05}$ is threshold for rejection of null hypothesis of zero coherency at 0.05 α-level.

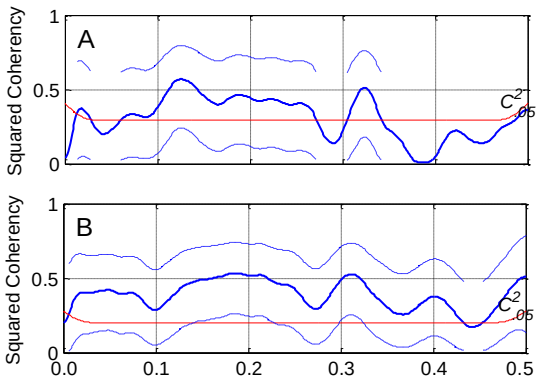

Figure A-11. Split-sample coherency analysis.

(A) Coherency spectrum of cross-spectral analysis the Virgin and Colorado Rivers for period, 1496 – 1700; (B) Coherency spectrum of cross-spectral analysis the Virgin and Colorado Rivers for period, 1700 – 2010.

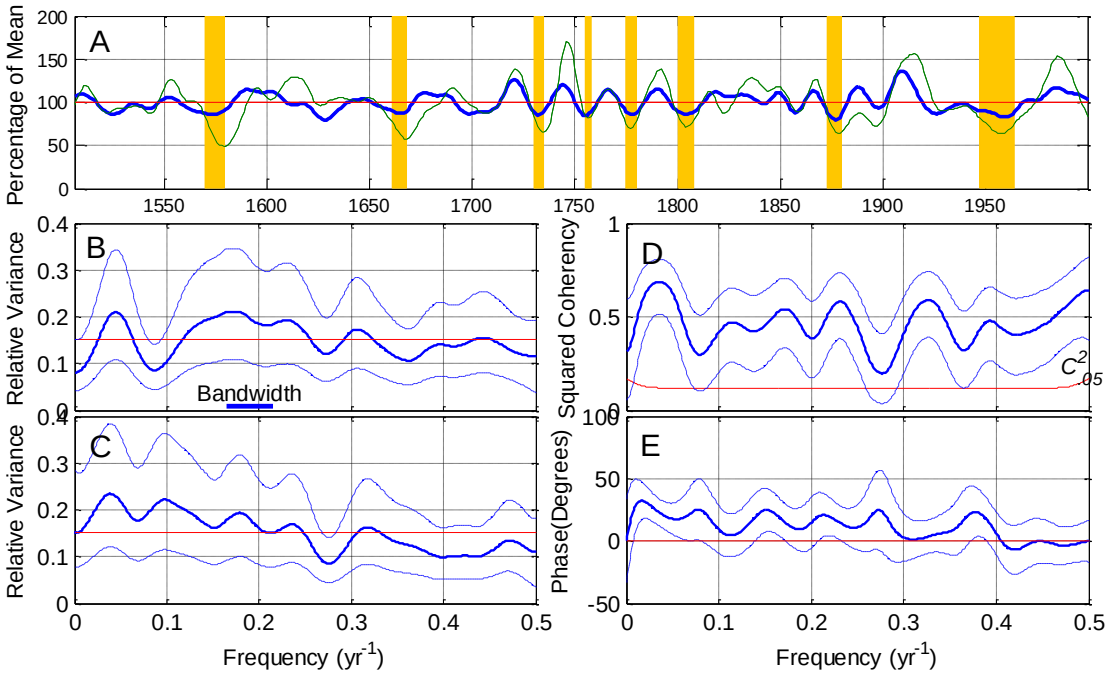

Figure A-12. Covariation of Virgin and Gila River reconstructed flows, 1496-2010

(A) Smoothed reconstructed flow series as percentage of long-term mean. Intervals with smoothed series simultaneously below 0.25 quantile shaded. Thick blue line is Virgin River; thin green line is Gila River. (B) Spectrum of Virgin. (C) Spectrum of Gila. (D) Coherency spectrum from cross-spectral analysis of Virgin and Gila. (E) Phase spectrum from the cross-spectral analysis. Smoothing in (A) by 21-year Gaussian filter. Confidence intervals (dashed) on spectral and cross-spectral plots are 95%. Line labeled $C^2_{.05}$ is threshold for rejection of null hypothesis of zero coherency at 0.05 α-level.

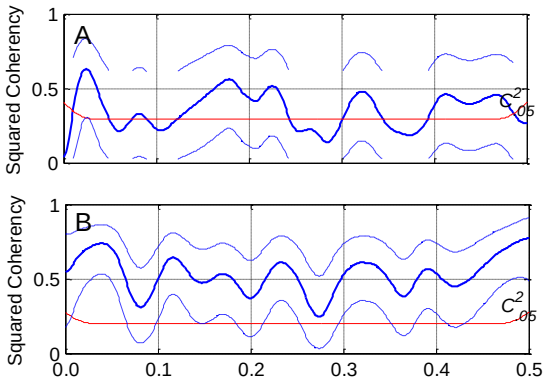

Figure A-13. Split-sample covariance.

(A) Coherency spectrum of cross-spectral analysis the Virgin and Gila Rivers for period, 1496 – 1700; (B) Coherency spectrum of cross-spectral analysis the Virgin and Gila Rivers for period, 1700 – 2010.